

Structural, morphological and electrochemical properties of novel $\text{Mg}_{1.8}\text{Mn}_{0.2}\text{Si}_{1-y}\text{Zr}_y\text{O}_4$ cathode material

S.B.R.S Adnan^{1,*}, S.H Tamin², M. Mustafa², N.S. Mohamed¹

¹ Centre for Foundation Studies in Science, University of Malaya, 50603 Kuala Lumpur, Malaysia

² Institute for Advanced Studies, University of Malaya, 50603 Kuala Lumpur, Malaysia

*E-mail: syed_bahari@um.edu.my

Received: 19 September 2019 / Accepted: 6 November 2019 / Published: 30 November 2019

$\text{Mg}_{1.8}\text{Mn}_{0.2}\text{Si}_{1-y}\text{O}_4\text{Zr}_y$, $0.0 \leq y \leq 0.4$ samples were prepared via sol gel method. The structural and electrochemical properties of the samples were systematically investigated. The diffraction peaks of the samples correspond to a single phase and indexed with an orthorhombic crystal system of space group *Pmna*. X-ray diffraction patterns of the materials showed no existing of impurities for $y \leq 0.3$ indicated that Zr^{4+} fully entered the lattice structure. Zr^{4+} doping influenced the enhancement of the structural and electrochemical performance of $\text{Mg}_{1.8}\text{Mn}_{0.2}\text{SiO}_4$. The substitution of Zr^{4+} with Si^{4+} in the lattice structure is expected to enhance the electron transfer in the structure by enlarge the migration channel of the compound. For this work, $\text{Mg}_{1.8}\text{Mn}_{0.2}\text{Si}_{0.7}\text{O}_4\text{Zr}_{0.3}$ which possessed the largest unit cell volume, a porous morphology and smallest R_{ct} , exhibits the smallest potential separation which contributed to the enhancement of electrochemical properties.

Keywords: Sol-gel; cathode; co-doped; electrode; magnesium ion battery.

1. INTRODUCTION

The expanding demand for large scale power system to meet various applications keep increasing [1, 2]. There is an urgent need to identify alternative cathode materials for developing rechargeable batteries which are cheap, safe and high energy. In the past few years, polyanion based materials with $(\text{XO}_4)^{n-}$ group have attracted considerable attention as cathode material in lithium ion batteries because of their safety and high stability [3]. Li_2MSiO_4 ($\text{M} = \text{Fe}, \text{Co}, \text{Ni}, \text{Mn}$) which is one of the polyanion based materials was a promising alternative cathode materials due to the order-disorder properties of atom without causing significant structural variation [4]. Meanwhile, this material also has high energy density with the ability to transfer two electrons per transition metal atom. The structural stabilities and multi-valent transition metal cores of these materials allow for reversible lithium ion insertion without much structural damage [5]. Various techniques have been adopted in Li ion battery research to enhance the

electrochemical performance of polyanion compounds such as particle size reduction [6-10], conductive carbon coating [11-17] and super valent cation doping [18-24].

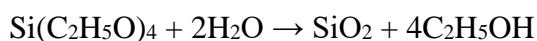
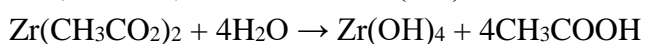
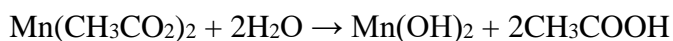
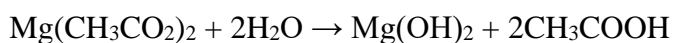
Recently, magnesium have attracted considerable attention in batteries system due to their safety and high abundance in nature [25-26]. However, development of magnesium based system have been hindered by two problems which are difficult to achieve reversible magnesium intercalation-deintercalation process and formation of passivation layer [3]. Following the achievement and development in polyanion based cathode materials for Lithium ion batteries and abundance of knowledge contributed, a huge attention has been given to the development of polyanion based cathode materials for magnesium ion batteries. A Forsterite compound, Mg_2SiO_4 has been proven to be a promising cathode material in magnesium rechargeable batteries [27]. A number of papers have been published on the modification of Mg_2SiO_4 in order to improve the electronic conductivity as well as its electrochemical activity in cathode material. M. Elhadri et al, have succeeded to modify the Mg_2SiO_4 structure by doped Ni^{2+} and Co^{2+} to the Mg^{2+} lattice site in solid solutions, $Mg_{2-x}Ni_x/Co_xSiO_4$ using the sol gel method [28]. Meanwhile, K. Mostafavi et al also have reported the modification of $Mg_2SiO_4 : Eu^{3+}$ [29] and $Mg_2SiO_4 : Dy^{3+}$ [30] using a combustion method and C. Shinho also has reported the modification of $Mg_2SiO_4 : Tb^{3+}$, Eu^{3+} [31] using solid state reaction method. The improvement of the electrochemical activity in the cathode material by elemental substitution of Mn^{2+} in $Mg_{2-x}Mn_xSiO_4$ solid solution using the sol gel method was discussed by our groups [32]. The potential interval (ΔV) was reported to decrease from 1.76 V in parent compound to 1.57 V in substituted compound indicated that, the doping is one of beneficial technique to enhance the performance of the Mg_2SiO_4 material [32].

The scope of the present work is to study the structural and electrochemical properties of novel $Mg_{1.8}Mn_{0.2}Si_{1-y}O_4Zr_y$ compound prepared by the sol-gel method. The substitution of Zr^{4+} with Si^{4+} in the lattice structure is expected to enlarge the migration channel of the compound. Detail studies on their structural and electrochemical properties were carried out since such study on this compound using this method has never been reported in the literature.

2. EXPERIMENTAL PROCEDURE

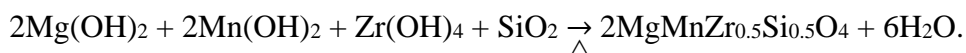
2.1 Preparation of $Mg_{1.8}Mn_{0.2}Si_{1-y}O_4Zr_y$ ($0.0 \leq y \leq 0.4$)

The $Mg_{1.8}Mn_{0.2}Zr_ySi_{1-y}O_4$ samples prepared in this study were synthesized using water-based citrate sol-gel method. Stoichiometric amounts of tetraethyl orthosilicate ($C_8H_{20}O_4Si$), TEOS, zirconium acetate tetrahydrate ($((CH_3.COO)Zr.4H_2O)$), manganese acetate tetrahydrate ($((CH_3.COO) Mn.4H_2O)$) and magnesium acetate tetrahydrate ($((CH_3COO)_2Mg.4H_2O)$) were used as starting materials while citric acid ($C_6H_8O_7$) used as the chelating agent. $(CH_3.COO)Zr.4H_2O$, $(CH_3.COO)Mn.4H_2O$, $(C_8H_{20}O_4Si)$ and $(CH_3COO)_2Mg.4H_2O$ were first dissolved in distilled water separately. Balance chemical reactions of the starting materials with water as described below:



Solution of each starting materials, including TEOS were then mixed to form a homogeneous

solution. Saturated aqueous solution of citric acid was slowly added to the solution under magnetic stirring. The solution was transferred into a reflux system and stirred at 70 °C until a clear pinkish solution was formed. The solution was evaporated at 80 °C to form a gel. The resulting wet gel was then dried in a vacuum oven at 150 °C for 24 hours. The obtained powder was ground and sintered at 1100 °C for 4 hours in a furnace. During sintering process, the balance chemical reactions for the compound is:



2.2. Materials characterization

PANalytical-X'pert³ X-ray diffractometer employing Cu K α radiation of wavelength of 1.5406 Å was used to identify the crystalline phase of the studied materials. Infrared spectra of Mg_{1.8}Mn_{0.2}Si_{1-y}O₄Zr_y (0.0 ≤ y ≤ 0.3) were recorded using a Perkin Elmer Frontier FTIR spectrometer in wavenumber range from 1350 to 550 cm⁻¹. The surface morphology was observed with a Zeiss-Evo MA10 scanning electron microscope. The particle size information was obtained using FRITTSCH-Analyssette 22 NanoTec laser particle analyzer. Impedance data were obtained by using Solatron 1260 impedance analyzer over a frequency range 1 to 10⁶ Hz. Transference number measurement was done using dc polarization method in order to determine the actual type of charge carriers in the obtained materials [33]. CV tests were performed using Wonatech ZIVE MP2 multichannel electrochemical workstation at a scan rate of 0.5 mV s⁻¹ on the potential interval – 2.0 to 5.0 V (vs. Mg²⁺/Mg). The reference and counter electrode were fabricated from magnesium metal. All tests were performed at room temperature.

3. RESULT AND DISCUSSION

Figure 1 shows the X-ray diffraction patterns of undoped Mg_{1.8}Mn_{0.2}SiO₄ and doped materials Mg_{1.8}Mn_{0.2}Si_{1-y}O₄Zr_y (0.1 ≤ y ≤ 0.3). All the peaks for doped sample fit the peaks for undoped structure very well without any impurity detected. All materials can be indexed on the basis of Forsterite, Mg₂SiO₄ and these sharp peaks in the pattern give an indication that the powders possess a high degree of crystallinity. The diffraction peaks of the samples correspond to a single phase and indexed based on Inorganic Chemistry Structure Database (ICSD) 98-008-8024 with an orthorhombic crystal system of space group *Pmna* (62). Compared with the XRD patterns of undoped Mg_{1.8}Mn_{0.2}SiO₄, all Zr doped samples have no extra reflection peaks detected in the XRD patterns for y ≤ 0.3. This indicates that Zr⁴⁺ entered the structure of Mg_{1.8}Mn_{0.2}SiO₄ rather than forming impurities. However, the increase of Zr⁴⁺ amount to 0.4 in Mg_{1.8}Mn_{0.2}Si_{1-y}O₄Zr_y compound resulted in the growth of impurity phase. Therefore, we decided not to do further characterizations on the Mg_{1.8}Mn_{0.2}Si_{0.6}O₄Zr_{0.4} sample.

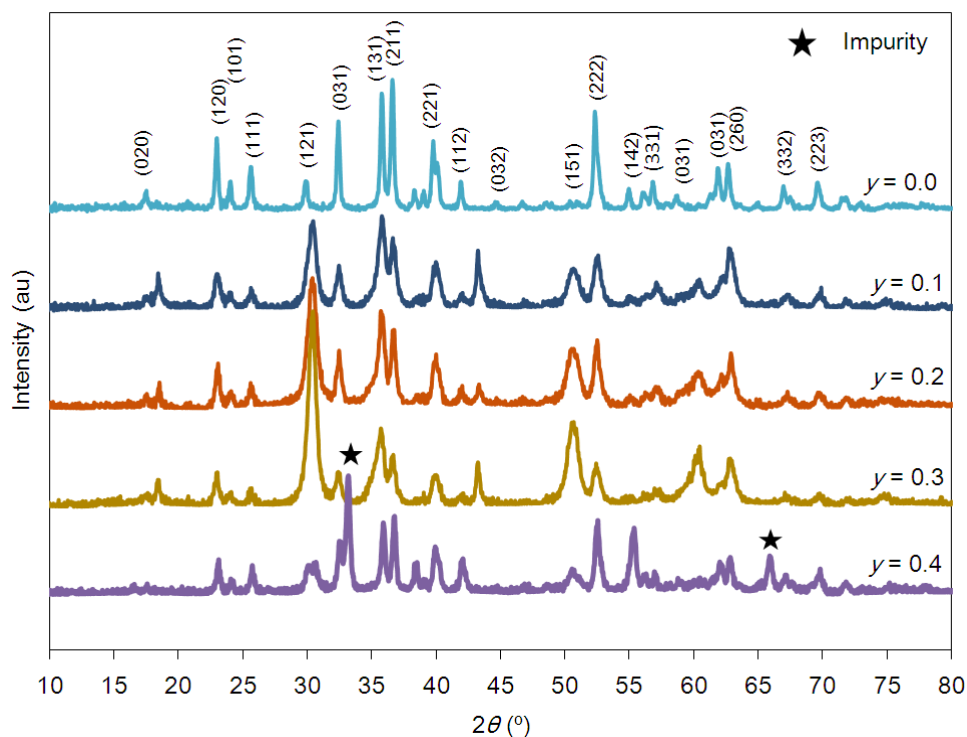


Figure 1. XRD pattern of $\text{Mg}_{1.8}\text{Mn}_{0.2}\text{Si}_{1-y}\text{O}_4\text{Zr}_y$ ($y = 0.0 - 0.3$).

The XRD spectra for $29.0^\circ \leq 2\theta \leq 32.0^\circ$ and $49.0^\circ \leq 2\theta \leq 52.0^\circ$ were magnified and illustrated in Figure 2. As can be seen in Figure 2(a), the dopant ratio from 0.1 to 0.3 leads to broadening of XRD peaks and a significant increase in their intensity. There is also a subtle but significant shift to the lower 2θ angle of the diffraction peaks in Figure 2(b). These observations prove that Zr^{4+} was successfully incorporated into the $\text{Mg}_{1.8}\text{Mn}_{0.2}\text{SiO}_4$ lattice without altering its structure for $0.0 \leq y \leq 0.3$. The occupation of dopant in the undoped lattice can be expected to result in small changes in the lattice parameters of the crystal structure.

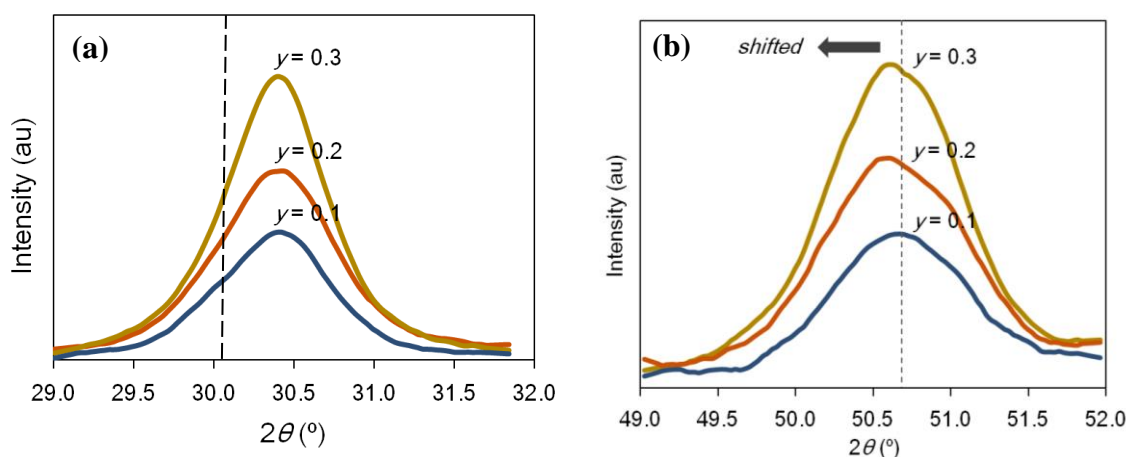


Figure 2. Extracted XRD patterns of $\text{Mg}_{1.8}\text{Mn}_{0.2}\text{Si}_{1-y}\text{O}_4\text{Zr}_y$ ($y = 0.1 - 0.3$) in the (a) $2\theta = 29.0^\circ - 32.0^\circ$ range and (b) $2\theta = 49.0^\circ - 52.0^\circ$ range.

The lattice parameters for $\text{Mg}_{1.8}\text{Mn}_{0.2}\text{Si}_{1-y}\text{O}_4\text{Zr}_y$ ($0.0 \leq y \leq 0.3$) samples were calculated using Bragg equation [34-35], and the results are listed in Table 1. As can be seen in Table 1, lattice parameter a increases with increasing of Zr^{4+} dopant amount. However, the changes in lattice parameters b and c are not monotonous. Lattice parameter b is the largest for sample $y = 0.2$ which is 6.1326 Å and the largest lattice parameter c is owned by sample $y = 0.3$ with 4.8351 Å. The unit cell volume shows the expansion, caused by the increase in lattice parameters, which may assist the intercalation and deintercalation of Mg ions during electrochemical processes. This increase in unit cell volume reveals the successful doping of Zr^{4+} into the structure.

Table 1. Lattice parameter of $\text{Mg}_{1.8}\text{Mn}_{0.2}\text{Si}_{1-y}\text{O}_4\text{Zr}_y$ ($y = 0.0 - 0.3$)

Sample $\text{Mg}_{1.8}\text{Mn}_{0.2}\text{Si}_{1-y}\text{O}_4\text{Zr}_y$	Lattice parameter			Volume of unit cell $V(\text{Å}^3)$	Crystallite Size (Å)
	a (Å)	b (Å)	c (Å)		
$y = 0.0$	10.0256	6.1249	4.7496	291.4208	25.59
$y = 0.1$	10.0190	6.1237	4.7499	291.6539	10.33
$y = 0.2$	10.0344	6.1324	4.7462	292.0528	10.82
$y = 0.3$	10.0417	6.1291	4.8351	297.5823	9.93

The observed changes is due to the replacement of the ionic radius or Zr^{4+} ion (0.72 Å) [35] is larger than ionic radius of Si^{4+} ion (0.41 Å). Similar method has been employed in previous works. Zr^{4+} doping has been used to stabilize and increase lattice parameter of olivine LiFePO_4 [35-37]. According to Scherrer's equation [38-39], the crystallite size of the undoped sample was calculated to be 25.59 Å while the crystallite size of the Zr^{4+} doped samples is in the range of 9.93 Å to 10.82 Å which is slightly smaller than that of the undoped $\text{Mg}_{1.8}\text{Mn}_{0.2}\text{SiO}_4$. This may be due to the small grain growth of Zr^{4+} doped materials compared to the undoped materials [40]. From the results above, we can conclude that the substituted of Zr^{4+} influenced the structural of $\text{Mg}_{1.8}\text{Mn}_{0.2}\text{SiO}_4$ compound.

FTIR spectra of $\text{Mg}_{1.8}\text{Mn}_{0.2}\text{Si}_{1-y}\text{O}_4\text{Zr}_y$ ($0.0 \leq y \leq 0.3$) system in a spectral region from 550 to 1350 cm^{-1} are shown in Figure 3. The FTIR spectra for $\text{Mg}_{2-x}\text{Mn}_x\text{Zr}_y\text{Si}_{1-y}\text{O}_4$ system are similar to that of magnesium silicate which contains five main characteristic peaks of $(\text{SiO}_4)^{4-}$ ion. There are peaks observed in the range of 550 - 650 cm^{-1} corresponding to SiO_4 bending vibration modes [41], peaks centered at 835 cm^{-1} and 874 cm^{-1} [42- 43] are assigned to symmetric stretching vibrations of Si-O-Si. Meanwhile, the characteristic peaks associated to SiO_4 stretching vibration modes are located in the range of 950 cm^{-1} to 990 cm^{-1} [41-43]. Lastly, the peaks appeared at 1105 cm^{-1} is attributed to Si-O-Si asymmetric stretching vibration mode of $\text{Mg}_{2-x}\text{Mn}_x\text{Zr}_y\text{Si}_{1-y}\text{O}_4$ [41-44]. Substituted Zr^{4+} into the $\text{Mg}_{1.8}\text{Mn}_{0.2}\text{SiO}_4$ structure shows a significant effect on the SiO_4 stretching vibration modes in the range of 950 cm^{-1} to 1050 cm^{-1} . The peaks for Zr^{4+} doped materials are broader compared to the characteristics peaks for undoped material. Inserted in Figure 4 clearly shows that SiO_4 stretching vibration peaks shifted to higher wavenumber. In addition, broadening of the shoulder peaks at 600 cm^{-1} to 750 cm^{-1} is also observed. The observed changes in the characteristic peaks prove that Zr^{4+} has an inductive

influence in lattice; this may introduce rearrangement of electric cloud in SiO_4^{4-} ion and is expected to enhance the electrochemical performance of the materials [45].

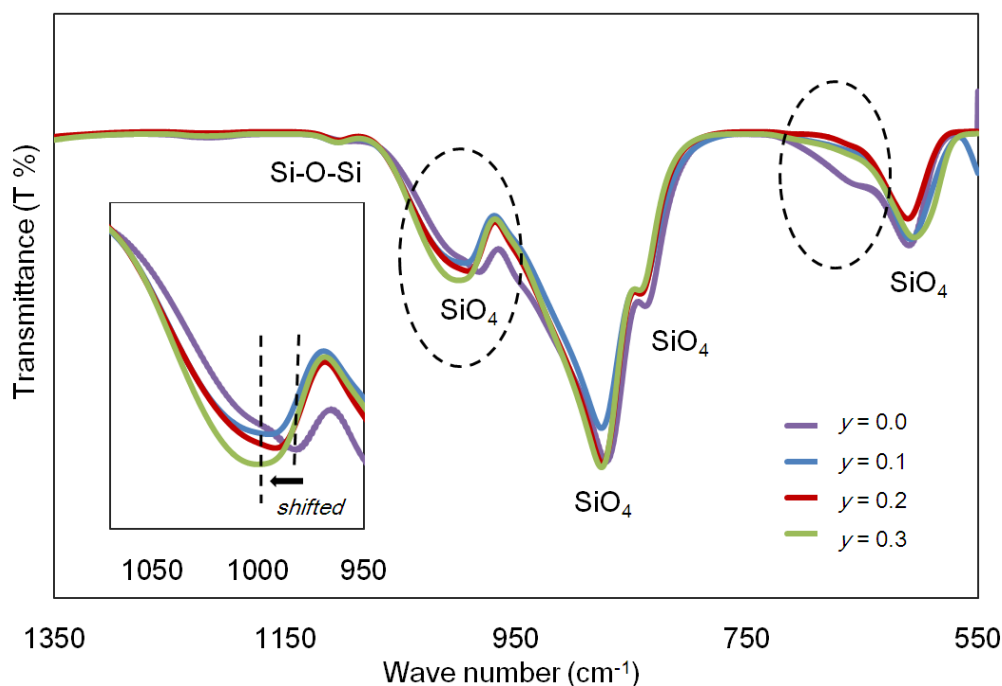


Figure 3. FTIR spectra of $\text{Mg}_{1.8}\text{Mn}_{0.2}\text{Si}_{1-y}\text{O}_4\text{Zr}_y$ ($y = 0.0 - 0.3$).

Scanning electron micrograph was performed to characterize the surface morphologies of the $\text{Mg}_{2-x}\text{Mn}_x\text{Zr}_y\text{Si}_{1-y}\text{O}_4$ samples. Figure 4 presents the SEM micrographs of $\text{Mg}_{1.8}\text{Mn}_{0.2}\text{Si}_{1-y}\text{O}_4\text{Zr}_y$ ($0.0 \leq y \leq 0.3$). From Figure 4 (a), it can be seen that the $\text{Mg}_{1.8}\text{Mn}_{0.2}\text{SiO}_4$ powders are uniform with small grains with sizes in micrometer range. The doped samples consist of agglomerated smaller particles that fused together and create a porous structure. Compared to the undoped material, Zr^{4+} doped samples contain loose and porous structure which is favorable for ion diffusion [46]. The morphology of the samples is almost insensitive to the dopant amount. However, the particle size analysis reveals that the average particle size increases with the increase of the dopant ratio. The average particle size is $17.30 \mu\text{m}$, $18.01 \mu\text{m}$, $19.24 \mu\text{m}$ and $22.65 \mu\text{m}$ for $y=0.0$, $y=0.1$, $y=0.2$ and $y=0.3$ respectively. Previous reports suggested that micron size particles have sufficient capacity to be used in electrochemical cell [47-48].

The details of ion migration were investigated by impedance method. Typical Nyquist plots of $\text{Mg}_{1.8}\text{Mn}_{0.2}\text{Si}_{1-y}\text{O}_4\text{Zr}_y$ ($0.0 \leq y \leq 0.3$) electrode obtained are presented in Figure 5. All profiles exhibit a semicircle in the high frequency region and a tilted spike in the low frequency region. The high frequency semicircle is related to the charge transfer process and the diameter of the semicircle is approximately equal to the charge transfer resistance (R_{ct}). The sloping line at low frequency is associated with the ion diffusion in solid phase [4]. Significant depressed semicircle is observed for samples with higher dopant compared to those with lower dopant indicating a marked decrease in R_{ct} . The lower R_{ct} implies that the materials possess easier charge transfer process [48-49]. Values of R_{ct} for all samples are presented in Table 2. Figure 6 shows the plot of normalized polarization current with respect to time for the highest conductivity sample, $\text{Mg}_{1.8}\text{Mn}_{0.2}\text{Si}_{0.7}\text{O}_4\text{Zr}_{0.3}$. The transference, t_{ele} for the sample is 0.41. This suggests

that this type of materials is a mixed conductor and thus suitable for use as cathode material in electrochemical cells.

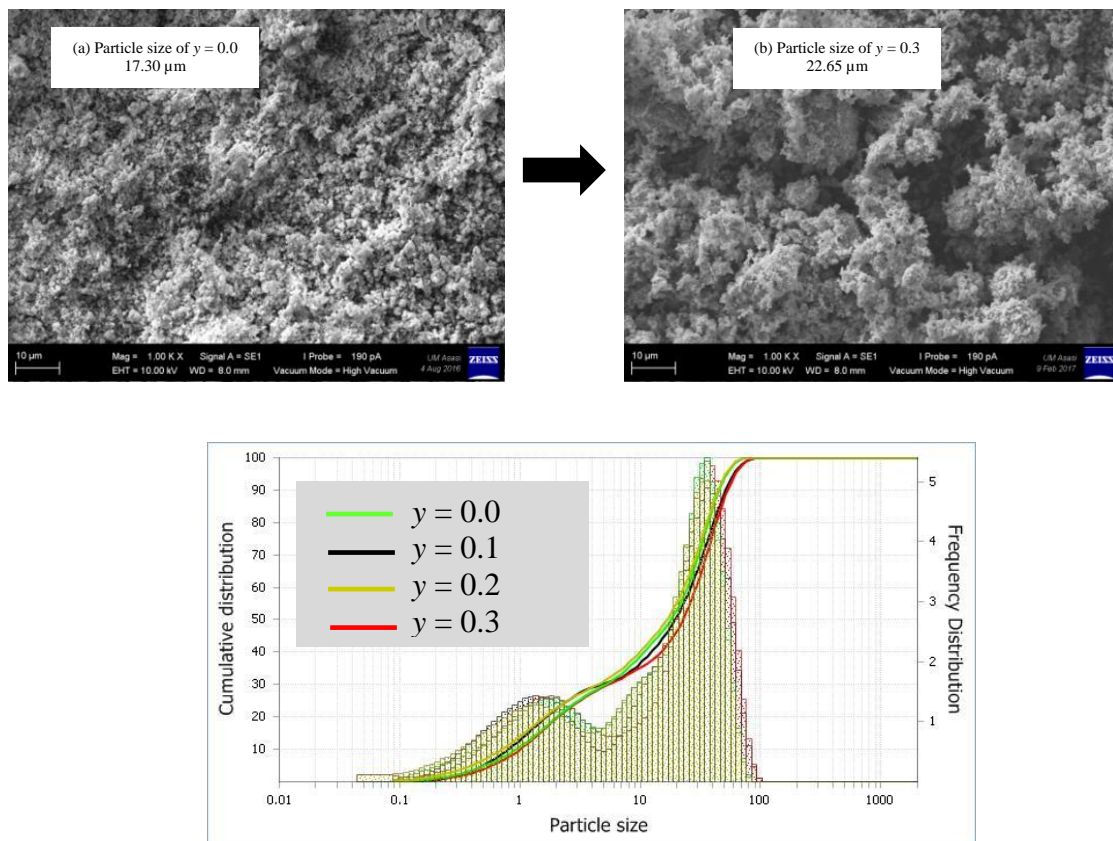


Figure 4. SEM images of (a) $y=0.0$ and (b) $y=0.3$ and particle size distributions of $Mg_{1.8}Mn_{0.2}Si_{1-y}O_4Zr_y$ with (a) $y=0.0$, (b) $y=0.1$, (c) $y=0.2$ and (d) $y=0.3$

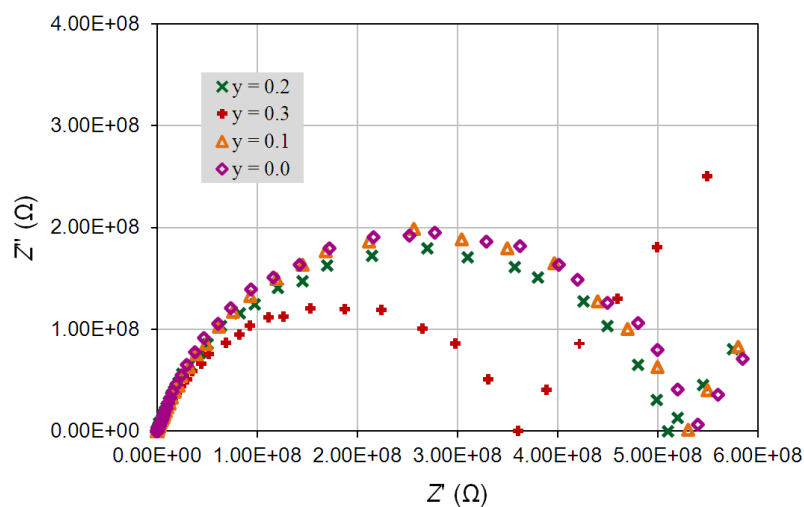


Figure 5. Nyquist plots of $Mg_{1.8}Mn_{0.2}Si_{1-y}O_4Zr_y$ with (a) $y=0.0$, (b) $y=0.1$, (c) $y=0.2$ and (d) $y=0.3$

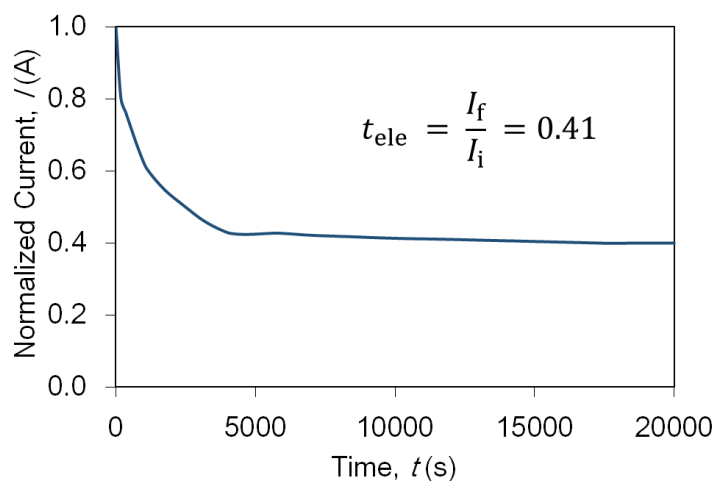


Figure 6. Current time curve of $\text{Mg}_{1.8}\text{Mn}_{0.2}\text{Si}_{0.7}\text{O}_4\text{Zr}_{0.3}$ sample

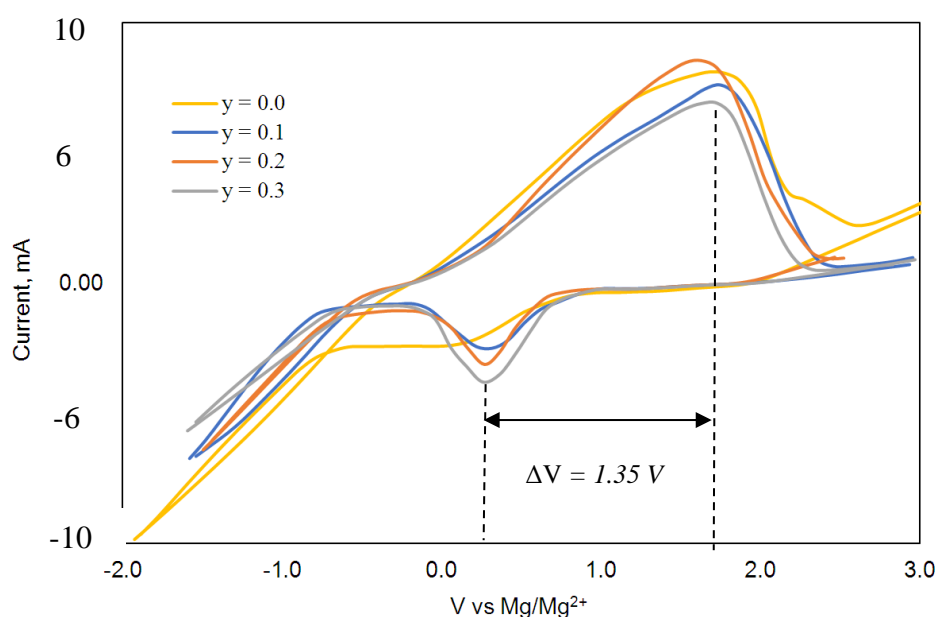
Cyclic Voltammetry (CV) analysis was used to investigate the electrochemistry of the $\text{Mg}_{1.8}\text{Mn}_{0.2}\text{Si}_{1-y}\text{O}_4\text{Zr}_y$ materials as a function of Zr^{4+} contents. Figure 7 depicts the CV curves of $\text{Mg}_{1.8}\text{Mn}_{0.2}\text{Si}_{1-y}\text{O}_4\text{Zr}_y$ ($y = 0.0 - 0.3$) system tested between -2.0 to 3.0 V at a scan rate 0.5 mVs^{-1} . All samples reveal similar CV curves with one pair of redox peak responds. It can be observed that the intensity of the peaks (anodic and cathodic) decreases with the increase of Zr^{4+} doping. Its indicate that, the substituted of Zr^{4+} in the $\text{Mg}_{1.8}\text{Mn}_{0.2}\text{Si}_{1-y}\text{O}_4\text{Zr}_y$ compound influenced the electron transfer. Meanwhile, the peak separation, ΔV of the doped samples is smaller compared to the undoped sample. The peak separation values for samples with dopant amount $y = 0.0$, $y = 0.1$, $y = 0.2$ and $y = 0.3$ are 1.67 V, 1.43 V, 1.36 V and 1.35 V respectively as shown in Table 2. This result is comparable with CV potential separation for some lithium polyanion based materials as listed in Table 3.

Table 2. Charge transfer resistance, R_{ct} and potential separation, ΔE for $\text{Mg}_{1.8}\text{Mn}_{0.2}\text{Si}_{1-y}\text{O}_4\text{Zr}_y$ ($y = 0.0 - 0.3$).

Sample $\text{Mg}_{1.8}\text{Mn}_{0.2}\text{Si}_{1-y}\text{O}_4\text{Zr}_y$	Charge transfer resistance R_{ct} (Ω)	Potential separation ΔV (V)
$y = 0.0$	5.83×10^8	1.67
$y = 0.1$	5.12×10^8	1.43
$y = 0.2$	5.34×10^8	1.36
$y = 0.3$	3.68×10^8	1.35

Table 3. CV potential separation of lithium polyanion based materials.

Materials	CV potential separation ΔV (V)	Ref.
$\text{Mg}_{1.8}\text{Mn}_{0.2}\text{Si}_{0.7}\text{O}_4\text{Zr}_{0.3}$	1.35	this work
$\text{Li}_2\text{FeSiO}_4$	0.80	[50]
Co doped $\text{Li}_2\text{FeSiO}_4/\text{C}$	1.53	[51]
$\text{Li}_2\text{CoSiO}_4$	0.50	[52]
$\text{Li}_2\text{MnSiO}_4/\text{C}$	1.55	[53]

**Figure 7.** Cyclic voltammograms of $\text{Mg}_{1.8}\text{Mn}_{0.2}\text{Si}_{1-y}\text{O}_4\text{Zr}_y$ with (a) $y = 0.0$, (b) $y = 0.1$, (c) $y = 0.2$ and (d) $y = 0.3$

For an electrochemical system, the potential separation between anodic and cathodic peaks reflects the reversibility of the electrochemical reaction. The potential separation between cathodic and anodic peak decreases as the dopant ratio increases. This is consistent with σ - y behavior. Therefore, it can be inferred that the potential separation in Figure 7 was improved by the influence of Zr^{4+} doping. This suggests that the performance of a sample is greatly improved upon Zr^{4+} doping process. $\text{Mg}_{1.8}\text{Mn}_{0.2}\text{Si}_{1-y}\text{O}_4\text{Zr}_y$ ($y = 0.3$) sample with cathodic-anodic peak located at 0.37/1.73 V exhibits the smallest potential separation which shows the improvement of electrochemical properties compared to undoped compound.

4. CONCLUSIONS

Pure $\text{Mg}_{1.8}\text{Mn}_{0.2}\text{Si}_{1-y}\text{O}_4\text{Zr}_y$ ($0.0 \leq y \leq 0.3$) were successfully synthesized via a water-based sol-gel method. The shift of XRD peak and FTIR peaks as well as the absence of extra reflection peaks in XRD spectra indicated that Zr^{4+} entered the structure of $\text{Mg}_{1.8}\text{Mn}_{0.2}\text{SiO}_4$ rather than forming impurities. Zr^{4+} doping resulted in enlarged unit cell volume. The increase in unit cell volume facilitates ion diffusion leading to enhancement in conductivity and intercalation/deintercalation process. Among all of the samples, $\text{Mg}_{1.8}\text{Mn}_{0.2}\text{Si}_{0.7}\text{O}_4\text{Zr}_{0.3}$ material shows the good electrochemical performance with possessed the largest unit cell volume, lowest R_{ct} value and most promising intercalation/deintercalation potential

ACKNOWLEDGMENTS

This work was supported by the University of Malaya financial through grants from University of Malaya RP013C-13AFR , RF003H-2018 and PG224-2015A. We also express gratitude to Ministry of Higher Education for scholarship My Brain15 awarded to Siti Hafizha.

References

1. Y. Orikasa, T. Masese, T. Koyama, T. Mori, M. Hattori, T. Masese, Y. Koyama, T. Mori, M. Hattori, K. Yamamoto, T. Okado, Z. D. Huang, T. Minato, C. Tassel, J. Kim, Y. Kobayashi, T. Abe, H. Kageyama, Y. Uchimoto, *Sci. Rep.*, 4 (2014) 5622.
2. M. M. Huie, D. C. Bock, E. S. Takeuchia, A. C. Marschiloka, K. J. Takeuchi, *Coordin. Chem. Rev.*, 15 (2015) 287.
3. Y. Li, Y. N. Nuli, J. Yang, T. Yiliner, J. L. Wang, *Chinese Sci. Bull.*, 56 (2011) 386.
4. H.-N. Girish and G.-Q. Shao, *RSV Advances*, 5 (2015) 98666.
5. M. M. Huie, D. C. Bock, E. S. Takeuchi, A. C. Marschiloka, K. J. Takeuchi, *Coordination Chemistry Reviews*, 287 (2015) 15.
6. C. Delacourta, P. Poizot, S. Levasseur, C. Masquelier, *Electrochemical and Solid-State Letters*, 9 (2006) A352.
7. R. Dominko, D. E. Conte, D. Hanzel, M. Gaberscek, J. Jamnik, *J. Power Sources*, 178 (2008) 842.
8. C. M. Julien, A. Mauger, K. Zaghib, *J. Mater. Chem.*, 21 (2011) 9955.
9. D. H. Kim, J. Kim, *Electrochemical and Solid-State Letters*, 9 (2006) A439.
10. D. H. Kim, J. Kim, *J. Phys. Chem. Solids*, 68 (2007) 734.
11. H. Huang, S. C. Yin, L. F. Nazar, *Electrochemical and Solid-State Letters*, 4 (2001) A170.
12. Z. L. Gong, Y. X. Li, G. N. He, J. Li, Y. Yang, *Electrochemical and Solid-State Letters*, 11 (2008) A60.
13. R. Dominko, M. Bele, M. Gabersceka, M. Remskar, D. Hanzel, S. Pejovnik, J. Jamnik, *J Electrochem. Soc.*, 152 (2005) A607.
14. M. R. Yang, T. H. Teng, S. H. Wu, *J. Power Sources*, 159 (2006) 307.
15. Y. Zhou, C. D. Gu, J. P. Zhou, L. J. Cheng, W. L. Liu, Y. Q. Qiao, X. L. Wang, J. P. Tu, *Electrochim Acta*, 56 (2011) 5054.
16. D. Lepage, C. Michot, G. Liang, M. Gauthier, S. B. Schougaard, *Angewandte Chemie - International Edition*, 50 (2011) 6884.
17. B. Peia, Q. Wang, W. Zhang, Z. Yang, M. Chen, *Electrochimica Acta*, 56 (2011) 5667.
18. S. Y. Chung, J. T. Bloking, Y. M. Chiang, *Nat. Mater.*, 1 (2002) 123.
19. M. S. Chen, S. H. Wu, W. K. Pang, *J. Power Sources*, 241 (2013) 690.
20. H. Liu, Q. Cao, L. J. Fu, C. Li, Y. P. Wu, H. Q. Wu, *Electrochem. Commun.*, 8 (2006) 1553.

21. Y. Wen, L. Zeng, Z. Tong, L. Nong, W. Wei, *J. Alloys Compd.*, 1-2 (2006) 206.
22. J. Ma, B. Lia, H. Du, C. Xua, F. Kang, *J. Electrochem. Soc.*, 158 (2011) A26.
23. C. S. Sun, Z. Zhou, Z. G. Xu, D. G. Wang, J. P. Wei, X. K. Bian, J. Yan, *J. Power Sources*, 193 (2009) 841.
24. J. Barker, M. Y. Saidi, J. L. Swoyer, *Electrochemical and Solid-State Letters*, 6 (2003) A53.
25. H. D. Yoo, I. Shterenberg, Y. Gofer, G. Gershinshy, N. Poura, D. Aurbach, *Energy & Environmental Science*, 6 (2013) 2265.
26. E. Levi, Y. Gofer, and D. Aurbach, *Chem. Mater.*, 22 (2009) 860.
27. S. H. Tamin, S. B. R. S. Adnan, M. H. Jaafar, N. S. Mohamed, *Ionics*, 24(9) (2018) 2665.
28. M. El Hadri, H. Ahamdane, M. A. El Idrissi Raghni, *Journal of the European Ceramic Society*, 35 (2015) 765.
29. K. Mostafavi, M. Ghahari, S. Baghshahi, A. M. Arabi, *Journal of Alloys and Compounds*, 555 (2013) 62.
30. M. Ghahari, K. Mostafavi, *Materials Research Bulletin*, 77 (2016) 48.
31. S. Cho, *Journal of the Korean Physical Society*, 69 (2016) 832.
32. S. H. Tamin, N. A. Dzulkarnain, S. B. R. S. Adnan, M. H. Jaafar, N. S. Mohamed, *Journal of Sol-Gel Science and Technology*, 86 (2018) 24.
33. P.G Bruce, J. Evans, C.A Vincent, *Solid State Ion.* 28 (1988) 918.
34. S. B. R. S. Adnan, N. S. Mohamed, *Ceram. Int.*, 40 (2014) 6373.
35. M. Wagemaker, B. L. Ellis, D. Lützenkirchen-Hecht, F. M. Mulder, L. F. Nazar, *Chem. Mat.*, 20 (2008) 6313.
36. H. Liu, C. Li, Q. Cao, Y. P. Wu, R. Holze, *J. Solid State Electrochem.*, 7-8 (2008) 1017.
37. N. Meethong, Y. Kao, S. A. Speakman, Y. Chiang, *Adv. Funct. Mat.*, 19 (2009) 1060.
38. B. D. Cullity, J. W. Weymouth, *Am. J. Phys.*, 25 (1957) 394.
39. N. Mustaffa, N. Mohamed, *Int. J. Electrochem. Sci.*, 10 (2015) 5382.
40. V. Mote, J. Dargad, B. Dole, *Nanoscience and Nanoengineering*, 1 (2013) 116.
41. A. Saber, B. Alinejad, Z. Negahdari, F. Kazemi, A. Almasi, *Mater. Res. Bull.*, 42 (2007) 666.
42. D. Mazza, M. Lucco-Borlera, G. Busca, A. Delasto, *J. Eur. Ceram. Soc.*, 11 (1993) 299.
43. M. Tsai, *J. Non-Cryst. Sol.*, 298 (2002) 116.
44. M. Kharaziha, M. Fathi, *Ceram. Int.*, 35 (2009) 2449.
45. H. Shu, X. Wang, Q. Wu, B. Hu, X. Yang, Q. Wei, Q. Liang, Y. Bai, M. Zhou, C. Wu, M. Chen, A. Wang, L. Jiang, *J. Power Sources*, 237 (2013) 149.
46. B. Lina, Z. Wena, Z. Gu, S. Huang, *J. Power Sources*, 175 (2008) 564.
47. K. Dokko, N. Nakata, K. Kanamura, *J. Power Sources*, 189 (2009) 783.
48. S. W. Oha, S. Myung, H. J. Bang, C. S. Yoon, K. Amine, Y. Suna, *Electrochem. Sol-State Lett.*, 12 (2009) A181.
49. L. Yang, L. L. Jiao, Y. Miao, H. Yuan, *J. Sol. State Electrochem.*, 14 (2014) 1001.
50. C. H. Hsu, Y. W. Shen, P. L. Kuo, L. H. Chien, *J. Nanoparticle Research*, 17 (2015) 54.
51. L. L. Zhang, S. Duan, X. L. Yang, G. Liang, Y. H. Huang, X. Z. Cao, J. Yang, M. Li, M. Croft, C. Lewis, *J. Power Sources*, 274 (2015) 194.
52. Z. L. Gong, Y. X. Li, Y. Yang, *J. Power Sources*, 174 (2007) 524.
53. M. Wang, M. Yang, L. Ma, X. Shen, *J. Nanomaterials*, 4 (2014) 1.